A coarse-grained model for DNA-functionalized spherical colloids, revisited: Effective pair potential from parallel replica simulations

Panagiotis E. Theodorakis, Christoph Dellago, and Gerhard Kahl

Citation: J. Chem. Phys. **138**, 025101 (2013); doi: 10.1063/1.4773920
View online: http://dx.doi.org/10.1063/1.4773920
View Table of Contents: http://jcp.aip.org/resource/1/JCPSA6/v138/i2
Published by the American Institute of Physics.

A coarse-grained model for DNA-functionalized spherical colloids, revisited: Effective pair potential from parallel replica simulations

Panagiotis E. Theodorakis,[1,2,3,a)] Christoph Dellago,[1,3] and Gerhard Kahl[2,3]
[1]*Faculty of Physics, University of Vienna, Boltzmanngasse 5, A-1090 Vienna, Austria*
[2]*Institute for Theoretical Physics, Vienna University of Technology, Wiedner Hauptstraße 8-10, A-1040 Vienna, Austria*
[3]*Center for Computational Materials Science (CMS), Wiedner Hauptstraße 8-10, A-1040 Vienna, Austria*

(Received 17 October 2012; accepted 17 December 2012; published online 10 January 2013)

We discuss a coarse-grained model recently proposed by Starr and Sciortino [J. Phys.: Condens. Matter **18**, L347 (2006)] for spherical particles functionalized with short single DNA strands. The model incorporates two key aspects of DNA hybridization, i.e., the specificity of binding between DNA bases and the strong directionality of hydrogen bonds. Here, we calculate the effective potential between two DNA-functionalized particles of equal size using a parallel replica protocol. We find that the transition from bonded to unbonded configurations takes place at considerably lower temperatures compared to those that were originally predicted using standard simulations in the canonical ensemble. We put particular focus on DNA-decorations of tetrahedral and octahedral symmetry, as they are promising candidates for the self-assembly into a single-component diamond structure. Increasing colloid size hinders hybridization of the DNA strands, in agreement with experimental findings. © *2013 American Institute of Physics*. [http://dx.doi.org/10.1063/1.4773920]

I. INTRODUCTION

Recent advances in nanotechnology aim at leading to the accurate design and manufacturing of materials with desired electronic, optical, and mechanical properties required for technological applications. However, realizing the full potential of nanotechnology requires a thorough understanding of how the basic building blocks of nano-materials self-assemble into structures of multiple length scales. DNA-functionalized nanometer- or micrometer-sized particles have recently attracted particular attention as a promising tool for controlled self-assembly of nano-materials.[1–3] The main goal would be the self-assembly of desired structures built of nano-particles linked by DNA.

It was first Mirkin *et al.*[4] and Alivisatos[5] who showed that DNA oligonucleotides can be efficiently grafted onto the surface of gold nano-particles to enable, by tuning the temperature, the reversible formation of larger rather amorphous assemblies. This work introduced the novel idea of using "encodable" interactions between particles based on bio-molecules[4–8] to direct the self-assembly process and create materials with novel properties. Possible applications of such materials include high-efficiency solar panels and lasers, super-resolution microscopes, or the fabrication of nano-composites of "metamaterials" with unusual electronic and optical properties; even coatings to render objects invisible have been discussed as a potential application of such nano-structures.[1,9–12] Oligonucleotide functionalized nano-particles have also found biological applications as they are used in diagnostic tools for nucleic acids and proteins,[14,15] intracellular probes,[16] and gene regulators,[17] to mention a few. However, it still remains a formidable challenge to take full benefit of self-assembly in order to manufacture novel magnetic, plasmonic and photonic metamaterials[9–12] of "long-range" ordered structures required for applications. For instance, long-range, quasi-crystalline structures composed of DNA-functionalized nanometer- or micrometer-sized particles' mechanical properties have not been realized, yet.[13]

In the work of Mirkin *et al.*[4] and Alivisatos[5] and subsequent experiments, mainly amorphous aggregates were obtained from DNA-coated particles, which could be classified as amorphous polymers.[7,18–28] Since then, various strategies towards crystallization were applied[29–31] in one and two dimensions. Finally, it was Nykypanchuk *et al.*[32] and Park *et al.*[33] who first reported crystalline structures in DNA-functionalized colloids. In their experiments, flexible spacers were grafted onto spherical particles with length of the order of the sphere diameter of the gold nano-particles. Crystallization took place at rather higher temperatures where the binding strands were dynamically and steadily forming double helices and dissociating back into single strands. The DNA macromolecules were grafted at random positions onto the surface of the spheres and over the entire surface of the gold nano-particle,[32,33] and the number of strands was varying from sphere to sphere as well. Nevertheless, these investigations along with subsequent work showed that in these self-assembly processes crystallization and lattice control were possible for face-centred-cubic (fcc) and body-centered-cubic (bcc) lattices by changing parameters such as the base sequence of the DNA or the overall oligonucleotide length.[7,21,28,32–37] The formation of different crystal structures can mainly be attributed to a competition between the entropic and enthalpic contributions, which are involved in the assembly process at different temperatures.

Recently, Macfarlane *et al.*[38] reported that gold nano-particle-DNA conjugates can be programmed to assemble

a)Electronic mail: panagiotis.theodorakis@univie.ac.at.

into various crystallographic structures. As discussed in these contributions, the use of single-stranded DNA as linkers might establish a general strategy to control the self-assembly of almost any nano-particle into a wide range of different periodic structures. Moreover, the authors proposed rules-of-thumb that can be used deliberately to prepare crystals with nine distinct space symmetries, in addition to fcc and bcc structures. In total, they determined the characteristics of 41 crystals and demonstrated that they had excellent control over lattice parameters on the 25–150-nanometers length scale: methods were presented to tune the lattice constant to basically any arbitrary value. However, still many issues remain open, the main one being related to the limited size of the crystalline structures, which are typically made of a few thousand nano-particles. Another approach to solve this problem discussed recently consists in attaching DNA to non-spherical nano-particles to create directional bonding enabling the realization of more complex structures.[39] In addition, in a follow-up work by the same authors, it has been shown how hollow DNA nano-structures can be used as "three-dimensional spacers" within nano-particle superlattices assembled through programmable DNA interactions.[40] Other approaches to direct the self-assembly of nano-materials have been also demonstrated, such as the use of Janus nano-particles functionalized with DNA molecules.[53]

Although crystalline structures have been achieved throughout for nanometer-sized particles, DNA programmed self-assembly has also been extended to particles of micrometer-scale size, such as in DNA-functionalized polystyrene microbead binary mixtures.[41] Occasionally, crystallites of close-packed, micrometer-sized particles have been reported.[7,28] However, the resulting structures do not lead to the same degree of order as observed for nanometer-size particles.[38]

A main focus of research in this field is the formation of diamond structures from DNA-coated colloids. This process is very important in colloidal crystallization[42] as the non-compact diamond lattice is essential for photonic crystals in the visible-light range.[43–49] However, although several methods have been proposed so far,[49–52] a successful single-component nano-particle assembly into a diamond structure has not been experimentally reported yet. Binary systems (where the two components differ, for instance, in the linkers), in which at least one component is arranged in a diamond lattice provide alternatives,[49,54,55] but the control of interparticle interactions is critical to this approach. A related theoretical prediction was made by Tkachenko,[52] who developed an effective potential acting between particles, showing that a diamond structure of single-component nano-particles is possible.

To assemble nano-particles with accuracy and reliable reproducibility is a very challenging goal. The major so far unresolved issue has been how to design materials displaying long-range order. In this endeavor, computer simulation can play a major role. To take into account all the interactions at a fully atomistic level in describing systems of few hundreds of DNA-functionalized particles is a rather formidable task. Thus, many different coarse-grained models have been put forward in recent years[56–72] yielding many important results, but none of these models have been able to propose a design for DNA-functionalized nano-particles capable of leading to the desired diamond structure. The sophistication of these models varies, depending on the particular aspects that the model tries to address. Recently, even models to capture the Hogsteen interactions between DNA bases beyond the Watson-Crick interactions have been proposed.[73] However, despite these efforts our theoretical understanding on the self-assembly of DNA-coated colloids remains limited.

In the present study, we revisit a recently proposed and, at first sight, simple coarse-grained model inspired by the so-called "bead-spring model"[74,75] widely used in polymer simulations.[76–86] This model has been proposed by Starr and Sciortino[63] and embodies two main aspects of DNA hybridization at the coarse-grained level. One is the bond specificity, which expresses the ability of bases to bond exactly to their complementary bases, i.e., Adenine ("A") can only form a hydrogen bond with Thymine ("T"), while Cytosine ("C") can only form a bond with Guanine ("G"). The second component of this model reflects in some way the nature of directionality of the hydrogen bonds, namely, once a base pair is formed no other base can establish a bond with a base that is already part of a bonded pair. The latter may be a strong approximation for some situations where some sequences can favor the formation of triple- and even four-stranded DNA structures.[87] An additional information that has to be encoded into the model is the fact that a double-DNA-helix exhibits a significantly higher persistence length (i.e., $\sim$50 nm, corresponding to $\sim$150 nucleotides[3]) to that of single-stranded-DNA (ssDNA) where the persistence length is $\sim$12 nucleotides. There is, however, some uncertainty on the exact value of the persistence length of ssDNA that also depends on solvent conditions. Roughly, the persistence length is about 4 nm[27,88] corresponding to 8–12 DNA bases.[13] In the model considered here, the stiffness even of the single strands is built in appropriately via a three-body angular interaction. This feature is justified by the fact that the present model will be used only for short DNA strands (4–16 nucleotides). From such a model, one is also able to extract the effective potential between two DNA-functionalized particles,[89,90] offering the possibility to simulate larger assemblies of DNA-functionalized particles. Based on the coarse-grained model, several studies have appeared in recent years leading to interesting conclusions on the formation of crystalline phases depending on the particular DNA sequences, decoration and size of the DNA-functionalized particles.[91–97] In these studies, crystallization has been observed for DNA-functionalized particles with octahedral symmetry, but, rather surprisingly, such conclusions are not drawn for the case of DNA-nano-particles with tetrahedral symmetry, which could be a very good candidate for diamond crystals given its symmetry. Therefore, it still remains a challenge to design these diamond structures exhibiting long-range order and possible enhancements on this simplistic model have to be considered in the future.

We have organized the present paper as follows. In Sec. II, we discuss in detail the model and the way to calculate the effective colloidal potential, as well as our simulation method. In Sec. III, we present representative results of

the effective potential calculation for different choices of the colloid size highlighting the main differences identified with respect to previous work. Finally, we summarize our conclusions in Sec. IV.

II. MODEL AND METHOD TO CALCULATE THE EFFECTIVE POTENTIAL

A. The model

The model put forward in Ref. 63 preserves the characteristic features of a standard bead-spring model for polymers[74,75] amended in such a way to incorporate two characteristic aspects of the DNA hydrogen bonds between complementary bases: first, the bond specificity of DNA bases and, second, the nature of the strong directionality of the hydrogen bond, i.e., one DNA base can bond with only one complementary DNA base. The latter, however, is a convenient assumption in various theoretical models as triple- and four-stranded DNA structures are also possible.[87] Furthermore, in the model of Starr and Sciortino[63] spherically symmetric potentials are considered throughout. Thus, any particular details of the underlying atomistic structure are not included at the coarse-grained level. Furthermore, the particle representing the core of a DNA-functionalized particle is assumed to have a spherical shape. The likewise spherical backbone beads represent the sugar/phosphate backbone along the DNA strands, and the smaller spherical base beads carry the information of the DNA bases. The mutual repulsion (or attraction) in pairs of DNAs is controlled by including (or suppressing) the attractive tail of the Lennard-Jones (LJ) potential in the interactions between pairs of DNA bases. As in the standard bead-spring model,[74,75] all beads interact with the standard LJ potential, cut and shifted at a cutoff distance r_c such that the potential and the force are continuous at r_c,

$$V(r) = V_{\mathrm{LJ}}(r) - V_{\mathrm{LJ}}(r_c) - (r - r_c)\left.\frac{dV_{\mathrm{LJ}}(r)}{dr}\right|_{r=r_c}, \quad (1)$$

where $V_{\mathrm{LJ}}(r)$ is the LJ potential

$$V_{\mathrm{LJ}}^{\alpha\beta}(r) = 4\varepsilon^{\alpha\beta}[(\sigma^{\alpha\beta}/r)^{12} - (\sigma^{\alpha\beta}/r)^{6}], \quad r \le r_c \quad (2)$$

with $\alpha, \beta = \mathrm{P}, \mathrm{B}, \mathrm{A}, \mathrm{C}, \mathrm{G}, \mathrm{T}$. The Greek superscripts α and β correspond to the different constituent entities of the DNA-functionalized nano-particle, where the letters P, B, A, C, G, and T refer to the core colloid particle (P), backbone beads (B), Adenine (A), Cytosine (C), Guanine (G), and Thymine (T), respectively.

We next define the particular interaction parameters between the colloid, the backbone, and the bases by defining the parameters $\varepsilon^{\alpha\beta}$ and $\sigma^{\alpha\beta}$. In this model, $\varepsilon^{\alpha\beta} = 1$ for all different combinations of α and β, setting also our units for energy. The Boltzmann constant is set to $k_{\mathrm{B}} = 1$ for convenience to define the temperature T in units of $\varepsilon^{\alpha\beta}/k_{\mathrm{B}}$. The size of the backbone beads is $\sigma^{\mathrm{BB}} = 1$, which is chosen as the unit of length; in contrast, the size for the bases is assumed to be $\sigma^{\mathrm{AA}} = \sigma^{\mathrm{CC}} = \sigma^{\mathrm{GG}} = \sigma^{\mathrm{TT}} = 0.35$; in all cases $\sigma^{\alpha\beta} = \sigma^{\beta\alpha}$ holds. For the colloidal particles, onto which the ssDNA strands are grafted, we have considered the following different values: $\sigma^{\mathrm{PP}} = 2$, 4, 8, 16, and 32.

The parameters $\sigma^{\alpha\beta}$ for the combinations $\alpha \neq \beta$ are defined according to the Lorentz-Berthelot rules [$\sigma^{\alpha\beta} = (\sigma^{\alpha\alpha} + \sigma^{\beta\beta})/2$, $\varepsilon^{\alpha\beta} = \sqrt{\varepsilon^{\alpha\alpha}\varepsilon^{\beta\beta}}$, therefore, $\varepsilon^{\alpha\beta} = 1$], with the only exception being $\sigma^{\mathrm{AB}} = \sigma^{\mathrm{CB}} = \sigma^{\mathrm{GB}} = \sigma^{\mathrm{TB}} = 0.35$. The latter choice has the effect that each base is almost completely contained within the shell of the backbone bead, thus, preventing the base from connecting to more than one complementary base.[63] In this way, the second aspect of this model mentioned above related to the nature of hydrogen bonds is fulfilled, although such an assumption may not hold in some cases.[87] However, it should be noted that the latter argument has been previously criticized by Knorowski *et al.*[72] for the model of Starr and Sciortino;[63] instead, the incorporation of additional flanking beads was suggested in order to ensure that artifacts, such as "hybridization" of three ssDNA or more, never occur in a multi-chain simulation. Since in the present study we will consider the model in the dilute limit, only two DNA-coated colloids will be involved in our calculations and consequently the above mentioned artifacts do not come into play.

The choice of the cutoff radius r_{c} determines whether the interaction potential will be attractive (by including the attractive tail of the LJ potential) or purely repulsive (when the latter is truncated at the minimum and shifted). In the present model, the attractive tail of the LJ potential is included for complementary bases, i.e., $r_{\mathrm{c}} = 2.5\sigma^{\mathrm{CG}} = 2.5\sigma^{\mathrm{AT}}$ while for any other interactions between beads α and β the cutoff radius is chosen to be $r_{\mathrm{c}} = 2^{1/6}\sigma^{\mathrm{AC}} = 2^{1/6}\sigma^{\mathrm{AG}} = 2^{1/6}\sigma^{\mathrm{CT}} = 2^{1/6}\sigma^{\mathrm{GT}}$, i.e., the interactions are purely repulsive. As a result, complementary bases are the only ones that attract each other via their attractive LJ tail. It should be noted that pairs of non-complementary bases interacting via the purely repulsive LJ potential do not really play a relevant role in the system since for these cases the base shell is fully incorporated in the backbone shell and it is rather the repulsive potential of the backbone beads that is relevant.

The potential specified in Eq. (1) acts between any pair of beads. In order to form bonds between beads, an additional $U_{\mathrm{FENE}}(r)$ potential[74,75] is introduced, given by

$$U_{\mathrm{FENE}} = -\frac{1}{2}kr_0^2 \ln[1 - (r/r_0)^2], \quad 0 < r < r_0, \quad (3)$$

where $U_{\mathrm{FENE}}(r \ge r_0) = \infty$; hence, r_0 is the maximal distance between bonded beads.[74,75] Specifically, the FENE potential acts between neighboring backbone beads and between each backbone bead and the base attached to it. The backbone beads attached to the colloidal particles are fixed at a given position on the surface of the colloid. As a consequence, when these backbone beads are selected to be moved within the Monte Carlo (MC) algorithm, the move is immediately rejected. However, if the colloidal particle is chosen for a move, the whole macromolecule is moved, preserving the positions of the beads within the reference frame, which is fixed at the center of the colloidal particle. In this way, the bonds between the colloidal particle and the first, grafted backbone beads are fixed. For all beads that interact via FENE potentials, the choice $r_0 = 1.5$ and $k = 30$ are used as in the standard bead-spring model,[74,75] resulting in an equilibrium average bond

length of ∼0.96 for $\sigma^{BB} = 1$.[74,75] This choice of parameters prevents crystallization in systems of polymeric chains.

Between the backbone beads and between the spherical colloidal particle and the beads grafted to its surface, a cosine-type bending potential acts between three neighboring beads along the same ssDNA defined as[99–101]

$$U_{\text{bend}}(\theta_i) = k_{\theta,\alpha\beta}[1 - \cos(\theta_i)]. \quad (4)$$

Here, $k_{\theta,\alpha\beta}$ is the elasticity parameter for beads of type α, β (with α, β = P or B); as suggested in the literature[63] a value $k_{\theta,\alpha\beta} = 5$ was assumed. It is worth noting that the choice of this value for the elasticity parameter is rather arbitrary, but it guarantees that a ssDNA chain is stiff enough, so that it does not interact with another ssDNA chain of the same particle. Experimental observations predict a 0.255 rise per base pair for dsDNA chains, which is very well reproduced in another model.[13] Also, the built-in stiffness of ssDNA in the model of Starr and Sciortino[63] excludes *a priori* the formation of hairpin[102] and loop[103] configurations, for example. In Eq. (4), $\cos(\theta_i) = \hat{\mathbf{r}}_{i,i-1} \cdot \hat{\mathbf{r}}_{i+1,i}$, where the unit vector $\hat{\mathbf{r}}_{i,i-1}$ points from the center of backbone bead $i-1$ to the center of the backbone bead i and $\hat{\mathbf{r}}_{i+1,i}$ is defined analogously.

When a DNA strand hybridizes with a complementary strand in a real system, the DNA double helix is formed and its stiffness is considerably larger than that of a ssDNA. Using the three-body potential specified in Eq. (4), the model guarantees that after DNA hybridization the two strands remain stiff. The artifact of this model is that this stiffness is already assumed *a priori* in the ssDNA strands. However, this assumption is not meaningless since this model was mainly suggested for short DNA strands where the length of the ssDNA is very small or of the same order compared to its persistence length and therefore the ssDNA strand can be considered as a "stick" in this model. One should point out that the use of the cosine-type potential in the model, Eq. (4), does not lead to a double helix structure after hybridization; it is rather only the bond specificity and the nature of the hydrogen bonds that this model tries to mimic in a reliable way. For more accurate descriptions of the mechanical properties of DNA, more complex models have been proposed in the literature (e.g., Refs. 56, 57, 65, and 66), where additional interactions have been included. In the present model, no potential other than the LJ and FENE potentials acts on the bases.

Finally, we come to the decoration of the colloidal particles. All strands attached to the colloidal particle have the same length, namely, eight bases, with sequence A-C-G-T-A-C-G-T (see Fig. 1(a)). In previous work, various geometries have been considered as potential and promising candidates for a single-diamond self-assembly scenario,[91–97] and particular emphasis was put on tetrahedral (cf. Fig. 2(b)) and octahedral symmetry (cf. Fig. 2(c)). In our investigations, we have mainly considered (i) the case where two interacting particles have either a tetrahedral (acronym "t-t") or an octahedral (acronym "o-o") decoration and (ii) the "mixed" case (acronym "t-o", where one colloid has a tetrahedral and the other one an octahedral decoration. Finally, also quadrangular-planar geometries (acronym "c-c") have been studied (see Fig. 2(a)).

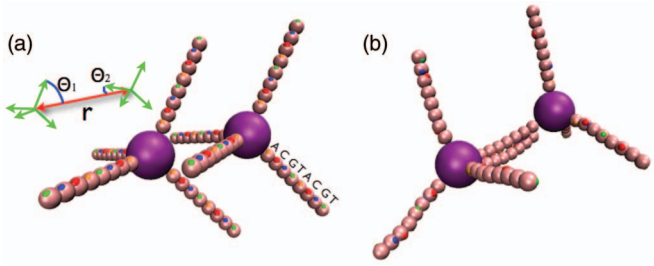

FIG. 1. Two spherical DNA-functionalized particles ($\sigma^{PP} = 4$) in the unbonded state are shown in panel (a). The DNA sequence for each strand is the same, namely, A-C-G-T-A-C-G-T (the bases are specified by differently colored spots on the beads). In this way, two strands can bind together palindromically in a bonded configuration, shown in panel (b). In addition, a schematic figure is shown on the left side of panel (a), where the definitions for the angles Θ_1 and Θ_2, as well as the distance r are specified (see main text). The green (or light gray) vectors are the ones that connect the respective centers of the colloids to the center of the first backbone monomer (attached to the colloid surface having an A-base), while the red (dark gray) bi-directional vector of length r links the centers of the two core colloids.

The model described above is illustrated schematically in Fig. 1, which shows for a tetrahedral geometry an initial structure used in our simulations (Fig. 1(a)) and a DNA-hybridized structure (Fig. 1(b)) resulting from the hybridization of the bases along one strand with the complementary bases of the other strand. Particles with this particular type of tetrahedral symmetry have raised much interest as promising building blocks for self-assembly into the diamond structure. The different colors of the small beads in Fig. 1 correspond to different types of bases. In the present study, as well as in previous studies based on this model,[91–97] the DNA sequence A-C-G-T is repeated along the DNA strand. In this way, two DNA sequences belonging to two different strands of two different functionalized colloids are thus palindromically favoring a particular bonded state, which is shown in Fig. 1(b).

B. Method to calculate the effective potential

An outline for the calculation of the effective potential acting between two DNA-functionalized nano-particles described within the model of Starr and Sciortino[63] has been presented earlier.[89] This method can be applied to systems where not only the distance between the two colloids has to be taken into account, but where also the direction between the arms of the particles is considered. As the model considers a spherical colloid with single and stiff DNA strands symmetrically grafted on it, we express the effective potential between two interacting DNA-functionalized colloids at a given

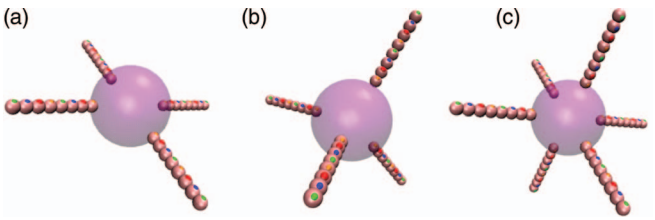

FIG. 2. Different decorations of DNA-functionalized particles with $\sigma^{PP} = 8$: A quadrangular planar (a), tetrahedral (b), and octahedral (c).

temperature as a function of the distance between the centers of the colloids and the relative orientations of the DNA strands. In this way, one obtains the probabilities to find the two particles at a given distance, and also the probability of having the DNA-arms oriented in a given direction.

A schematic representation of the geometrical quantities used for the calculation of the effective potential is given in Fig. 1. The distance between the centers of the colloids is denoted as r. The direction of the DNA strands on each of the two colloids (denoted as 1 and 2) are expressed via the angles Θ_1 and Θ_2 and illustrated in Fig. 1: Θ_1 is the angle that a DNA strand attached to colloid 1 forms with the line connecting the two colloid centers; only the arm located closest to this vector is considered. Correspondingly, one defines angle Θ_2 for the DNA-functionalized colloid 2. Here, the direction of the colloids is defined through the vector connecting the center of the colloid with the first backbone bead attached to the colloid. Furthermore, we have verified that the dihedral angle spanned by vectors connecting the colloid centers with the respective anchoring points of the DNA-strands and the vector connecting the center of the two colloids is uniformly distributed both in bonded and unbonded states. As a consequence, there are no effective interactions acting on this degree of freedom.

One now has to define a criterion when two DNA strands are considered to be bonded: (i) two bases are defined as bonded if they belong to different strands and are separated by a distance smaller than $2.5\sigma^{\mathrm{AA}}$; (ii) furthermore – as has been stated previously[63,89] – two DNA strands are considered bonded when half or more of the DNA bases of the strand are bonded with the bases of the other strand. An alternative criterion has also been discussed,[90] namely, two molecules are bonded if their bonding energy is lower than -0.4. We have verified that the choice of the value of the energy or the distance criterion does not affect the final result for the effective potential obtained here.

In Refs. 63 and 89, it has been suggested that the effective potential can be defined as a linear combination of two states, i.e., the bonded state in which two strands are bonded as defined above (for example, see Fig. 1(b)) and the unbonded state, in which they are not bonded. Then, the probability $p_b = p_b(T)$ of two strands to be bonded can be readily computed by counting during the simulation how many configurations correspond to the bonded and unbonded state, respectively. The role of temperature is to modify this probability: at lower temperatures, two strands spend more time in a bonded state; as the temperature is increased, bonded configurations become rarer until they eventually disappear. As will be shown below, the values of the probability p_b can be fitted within a two state model. Then, the probability of the particles to be separated by a certain distance r is described by the following expression:

$$P(r) = p_b(T)P^{\mathrm{bonded}}(r) + [1 - p_b(T)]P^{\mathrm{unbonded}}(r), \quad (5)$$

i.e., the probability of two DNA-functionalized colloids being separated by a distance r is a linear combination of the respective probabilities for bonded and unbonded configurations, $P^{\mathrm{bonded}}(r)$ and $P^{\mathrm{unbonded}}(r)$. These probabilities are defined such that $\frac{4\pi}{V}\int P(r)r^2dr = 1$ with V being the volume of the simulation box.

These probabilities are nothing else than the radial distribution functions which are measured in bonded $[P^{\mathrm{bonded}}(r)]$ and unbonded states $[P^{\mathrm{unbonded}}(r)]$. Accordingly, the contribution of the two probabilities, $P^{\mathrm{bonded}}(r)$ and $P^{\mathrm{unbonded}}(r)$, to $P(r)$ is weighted by the probabilities of two DNA strands to be bonded $p_b(T)$ or unbonded $[1 - p_b(T)]$; the temperature dependence is purely taken into account via $p_b(T)$. Consequently, an accurate determination of the probability p_b plays a pivotal role in the calculation of the effective potential. The assumption that $P(r)$ can be computed as a linear combination of $P^{\mathrm{bonded}}(r)$ and $P^{\mathrm{unbonded}}(r)$ weighted via p_b and $(1 - p_b)$ has been confirmed by determining the radial distribution function of two interacting DNA-coated colloids at different temperatures.[89]

In the next step, one has to determine the probability $P(\Theta_1, \Theta_2)$, which accounts for the orientations of the ssDNA strands in the calculation of the effective potentials. Again, index 1 labels colloid 1, while 2 indicates colloid 2. An important assumption within this model is that the orientations of the two DNA strands involved are independent in both bonded and unbonded cases. Although this assumption seems to be strong, it has been confirmed.[89] Consequently, the joint probability to observe angles Θ_1 and Θ_2 can be written as the product of two independent probabilities,

$$P(\Theta_1, \Theta_2) = P(\Theta_1)P(\Theta_2). \quad (6)$$

We have computed joint probabilities of the angles Θ_1 and Θ_2 and have verified that these two angles are indeed statistically independent even in the bonded state. Here, $P(\Theta_1)$ and $P(\Theta_2)$ are normalized such that $\frac{1}{2}\int_0^\pi P(\Theta_i)\sin\Theta_i d\Theta_i = 1$, $i = 1, 2$. In a similar manner as for the probability $P(r)$ it has been assumed[89] that the respective probabilities for the angles Θ_1 and Θ_2 can be expressed as a linear combination of the respective distributions in the bonded and unbonded states. Thus,

$$P(\Theta_i) = p_b(T)P^{\mathrm{bonded}}(\Theta_i) + [1 - p_b(T)]P^{\mathrm{unbonded}}(\Theta_i), \quad i = 1, 2. \quad (7)$$

In other words, one can split up the probability of finding two particles at a given distance r with given directions of their DNA-arms, as a linear combination of the probabilities in the bonded or unbonded states, weighted by the probability $p_b(T)$ and $[1 - p_b(T)]$.

Finally, the total normalized probability of finding two colloids at a distance r and their nearest arms at angles Θ_1 and Θ_2 reads

$$P(r, \Theta_1, \Theta_2) = p_b P^{\mathrm{bonded}}(r, \Theta_1, \Theta_2) + (1 - p_b)P^{\mathrm{unbonded}}(r, \Theta_1, \Theta_2), \quad (8)$$

where

$$P^{\lambda}(r, \Theta_1, \Theta_2) = P^{\lambda}(r)P^{\lambda}(\Theta_1)P^{\lambda}(\Theta_2) \quad (9)$$

and $\lambda =$ unbonded, bonded. For unbonded configurations, one assumes that all directions of the DNA strands are equally

likely, leading to the normalized angular distribution

$$P^{\text{unbonded}}(\Theta_i) = 1, \tag{10}$$

where $i = 1, 2$. Distributions of the angles Θ_1 and Θ_2 are of this form for sufficiently large radial distances where the excluded volume for one molecule due to the presence of the other particle is negligible. For smaller distances, however, bigger angles should be favored and Eq. (10) is not strictly valid in this regime.

For the unbonded configurations, the joint probability $P^{\text{unbonded}}(\Theta_1, \Theta_2)$ is then given by

$$P^{\text{unbonded}}(\Theta_1, \Theta_2) = 1. \tag{11}$$

In the case of bonded configurations, it is assumed that the probability for a given Θ_i ($i = 1, 2$) is independent of the radial distance; in the bonded state, this radial distance varies slightly around the average distance between the centers of the colloids. It has been shown[89] – and we also confirm this observation in the present contribution – that the probability $P^{\text{bonded}}(\Theta_i)$ can be fitted well to a Gaussian function, namely,

$$P^{\text{bonded}}(\Theta_i) = \frac{A}{\sqrt{2\pi s^2}} \exp\left(-\frac{\Theta_i^2}{2s^2}\right), \tag{12}$$

where A is a normalization constant. Thus, the joint probability for Θ_1 and Θ_2 can be written as a product of two independent Gaussian functions,

$$\begin{aligned} P^{\text{bonded}}(\Theta_1, \Theta_2) &= \frac{A}{\sqrt{2\pi s^2}} \exp\left(-\frac{\Theta_1^2}{2s^2}\right) \frac{A}{\sqrt{2\pi s^2}} \exp\left(-\frac{\Theta_2^2}{2s^2}\right) \\ &= \frac{A^2}{2\pi s^2} \exp\left(-\frac{\Theta_1^2 + \Theta_2^2}{2s^2}\right). \end{aligned} \tag{13}$$

The full probability can then be written [(Eq. (9)] as

$$\begin{aligned} P(r, \Theta_1, \Theta_2, T) = {} & p_b(T) P^{\text{bonded}}(r) P^{\text{bonded}}(\Theta_1, \Theta_2) \\ & + [1 - p_b(T)] P^{\text{unbonded}}(r). \end{aligned} \tag{14}$$

Finally, the effective potential, $V^{\text{eff}}(r, \Theta_1, \Theta_2)$, is obtained from the above probabilities via

$$\beta V^{\text{eff}}(r, \Theta_1, \Theta_2, T) = -\ln[P(r, \Theta_1, \Theta_2, T)]. \tag{15}$$

Within this formalism, the repulsive part of the potential has been spherically averaged. Of course, this is only an approximation to the real situation, and as the particles move away from each other, this approximation becomes more accurate. The main reason for choosing this way of dividing configurations in bonded and unbonded states is to guarantee the continuity of the effective potential. At the same time, one avoids configurations in which strands are partially bonded with respect to the definition of bonded and unbonded configurations (cf. Fig. 1).

C. Simulation method

In order to calculate the effective potential within this model,[63] we first performed standard MC simulations in the canonical ensemble in a cubic simulation box with periodic boundary conditions: the total number of beads, N, the volume of the simulation box V, and the temperature T are constant while the energy E is allowed to fluctuate. The length of the box $L = V^{1/3}$ is sufficiently large that two colloids do not interact with any of their periodic images (cf. Table I). We note here that an increase of the size of the simulation box results in an increase of the entropy of the unbonded state (the number of unbonded states increases with the size of the box). Therefore, we strictly choose the smallest possible box to simulate our systems in order to minimize such an effect. We have considered three different types of MC moves:

TABLE I. Side length L of the cubic simulation box in units of σ^{BB} used in our simulations for different decorations and colloid sizes as indicated.

	L		
Decoration	$\sigma^{\text{PP}} = 2$	$\sigma^{\text{PP}} = 4$	$\sigma^{\text{PP}} = 8$
t-t	26	32	38
t-o	32	36	44
o-o	38	42	50

(i) Standard local bead moves, in which N attempts to move at random a randomly chosen bead are performed. When beads that are tethered to the colloidal surface are selected for a move, this attempt is directly rejected. In this way, the beads which are grafted on the surface of the colloid are not able to slide on the colloid surface, but remain fixed at the specific grafting point.

(ii) The second type of move involves N_m attempts (in our case $N_m = 2$, as we simulate only two macromolecules) to rotate a randomly selected colloid by a random angle. For this pivot move the centre of the colloid particle is taken as reference point.

(iii) The third move corresponds to $N_m = 2$ attempts to select one of the two colloids at random and translate it as a whole as in a usual local move. In such a move, the colloidal particle and all beads belonging to it are moved by the same displacement.

The combination of the three moves, each of them realized once, defines a MC step. The acceptance or rejection of a new configuration is decided as usual via the standard Metropolis criterion.[104]

For reasons which will become apparent below, we have found it indispensable to use the parallel tempering method[105–107] to compute the effective potential between two colloids. In a parallel tempering simulation,[107] one considers M replicas, each representing a canonical ensemble, at a different temperature, T_i. In our simulations, we have typically used about 60 different temperatures. The different simulation temperatures should be chosen such that the histograms of the fluctuating energies of adjacent replicas overlap; in this way, the exchange of temperatures or configurations between two adjacent replicas (i.e., between the configurations at temperatures T_i and T_{i+1}) takes place at a sufficient rate. Different approaches on how to select the different temperatures have been discussed.[108–110] We point out that generally a rather dense selection of temperatures is required at lower temperatures where energy fluctuations are suppressed leading to a small overlap of adjacent energy histograms. Since the replicas do not interact energetically, the partition function of this

total ensemble of M replicas can be expressed as the product of the canonical partition functions. Moves in the temperature space between ensembles i and j are accepted with probability

$$P_{\text{acc}} = \min\left\{1, \exp\left[(\beta_i - \beta_j)\left(V\left(\mathbf{r}_i^N\right) - V\left(\mathbf{r}_j^N\right)\right)\right]\right\}, \quad (16)$$

where $V(\mathbf{r}_i^N)$ is the total energy of the system at configuration $\mathbf{r}_i^N$. Swaps are normally attempted between systems with adjacent temperatures, $j = i + 1$. To satisfy detailed balance, the swap moves must be performed with a certain probability, and performing the swaps after a fixed number of single-temperature MC moves satisfies the sufficient condition of balance.[111] In our simulations, we have tried many different combinations of the number of swap moves. The results shown here are taken by attempting a swap move every 50 MC steps between a replica at temperature T_i and a replica at the higher, adjacent temperature T_{i+1}.

In order to implement this protocol we have developed a parallel code implementing the Message Passing Interface, where each replica running at different temperature T_i is assigned to a different processor. The total number of MC steps we performed for each studied case amounts to 5×10^8 MC steps, while properties are measured after equilibrium has been achieved for a total of 3×10^4 samples which are collected every 5×10^3 MC steps. This large number of samples is required for an accurate calculation of the probability $P^{\text{bonded}}(\Theta_1, \Theta_2)$, while the calculation of $P(r)$ requires less effort. Overall, the determination of the effective interaction between two DNA-coated colloids is computationally very expensive.

III. RESULTS

A. The system

We have implemented the MC simulation method outlined in Sec. II C to calculate the effective potential between DNA-functionalized spherical colloids.

While in previous studies[91–97] DNA-strands with 4–16 bases were considered, we have restricted ourselves in the present study to $N_b = 8$ bases, their sequence being A-C-G-T-A-C-G-T (cf. Fig. 1(a)); all strands attached to the colloidal particles have the same length. In an effort to study the impact of the size of the colloid, we have varied the colloidal diameter, σ^{PP}, over a representative set, assuming the following values: $\sigma^{\text{PP}} = 2$, 4, 8, 16, and 32.

B. Evaluation of $p_b(T)$

Our first attempts to evaluate the effective potential between two DNA-decorated colloidal particles were carried out in a series of standard simulations in the canonical ensemble, where runs at different temperatures are carried out independently, starting from a random, unbonded configuration. As the simulations are carried out at each temperature independently, the DNA strands will form bonds – in particular, as a consequence of the cosine potential Eq. (4) – only at sufficiently low temperatures (i.e., for $T \leq 0.11$). As documented in the literature[63,89] and confirmed by our investigations, the transition from unbonded to bonded configurations takes place in a very narrow temperature range, i.e., $0.09 \leq T \leq 0.11$. In this interval, a decay of $p_b(T)$ could be observed, which can be fitted in a two-state model via the expression

$$p_b(T) = \frac{1}{1 + e^{-(\Delta E/T - \Delta S)}}, \quad (17)$$

where $\Delta E = E_u - E_b$ and $\Delta S = S_u - S_b$ are the energy and entropy differences between unbonded (index "u") and bonded states (index "b"), respectively.

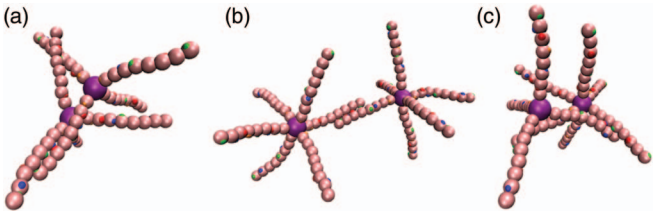

FIG. 3. Different anomalously bonded (they are not strictly bonded according to the definitions specified in the main text) configurations of two interacting DNA-functionalized colloids, obtained during a standard simulation in the canonical ensemble at a fixed temperature starting from an unbonded configuration (see Fig. 1(a)). Below $T \approx 0.09$ the systems can hardly change from such a bonded state to a lower energy state during the calculation of the effective potential. Characteristic configurations for tetrahedral-tetrahedral geometry (t-t – panel (a)) at temperature $T = 0.061$, octahedral-octahedral (o-o – panel (b)) at $T = 0.069$, and tetrahedral-octahedral (t-o – panel (c)) at $T = 0.065$ are shown. In all cases, the size of the colloidal particle was assumed to be $\sigma^{\text{PP}} = 2$. Similar structures arise for values of σ^{PP} up to 16. Such configurations also survive within the temperature range $0.09 < T < 0.11$. For $T > 0.11$ only unbonded configurations are observed.

In our investigations, based on standard canonical simulation, we have found that bonded configurations (according to our definition – e.g., see Fig. 1(b)) are observed that cannot be considered as favorable: in particular in the temperature range $0.09 \leq T \leq 0.11$, also other "unfavorable" (partially bonded) configurations are observed (Fig. 3). Of course, such configurations are an artifact of the model and cannot form in reality, since in these cases (Figs. 3(a) and 3(b)) strands are attached using their 5′ end. In addition, in standard canonical MC simulations, transitions from one configuration to another can hardly take place at low temperatures leading to frozen configurations that do not change anymore. This ergodicity problem is also observed in the original data corresponding to the transition regime of bonded and unbonded configurations,[63] where one can recognize the difficulty for efficient sampling in the transition regime of $p_b(T)$.

The occurrence of such problems in two-state systems in narrow temperature ranges is well known in a wide variety of systems and its solution represents a challenge for computer simulations.[98] To improve the sampling of configuration space, we have therefore implemented a parallel tempering scheme described in Subsection II C. As will be discussed below, this parallel tempering approach yields a significantly lower transition temperature from the bonded to the unbonded state and a considerably broader transition range in temperature compared to the results of Starr *et al.*[63,89]

In Fig. 4, we present results for the probability $p_b(T)$ as a function of temperature as obtained from the parallel tempering simulation scheme, for different values of the colloidal size, σ^{PP}, and different decorations. The observed transition

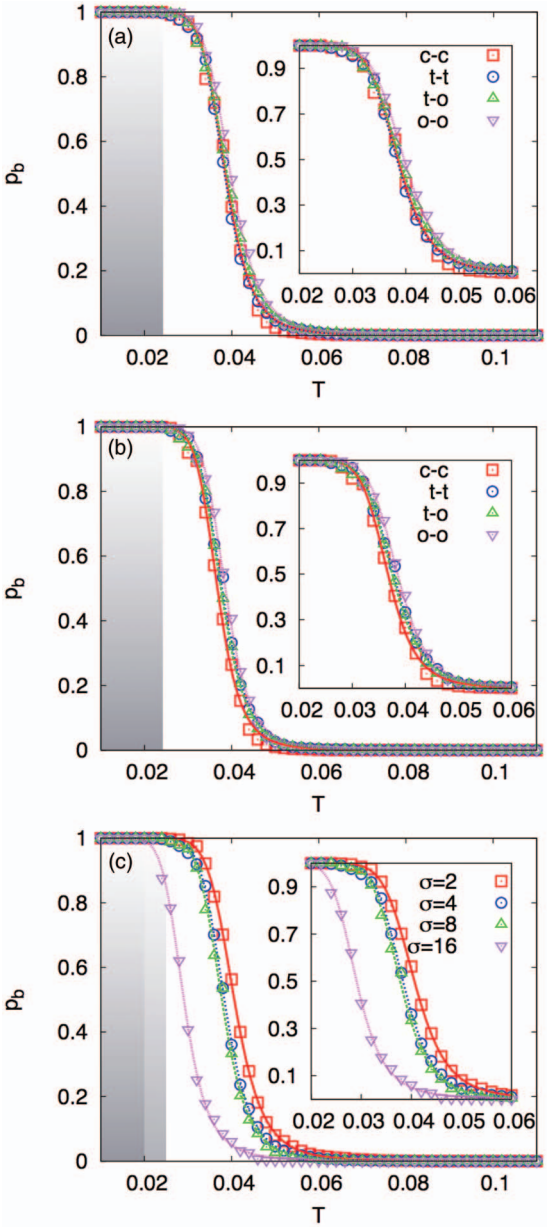

FIG. 4. The probability $p_b(T)$ of finding a bonded configuration (as the one shown in Fig. 1(b)) for different DNA decorations. Panel (a) shows results for $\sigma^{PP} = 4$ for quadrangular-planar-quadrangular-planar (c-c), tetrahedral-tetrahedral (t-t), tetrahedral-octahedral (t-o), and octahedral-octahedral geometry (o-o). Panel (b): Same as panel (a), but for $\sigma^{PP} = 8$. Panel (c) shows results for the tetrahedral-tetrahedral case (cf. Figs. 1(a) and 1(b)) for different colloid sizes, i.e., $\sigma = \sigma^{PP} = 2$, 4, 8 and 16 (as labeled). Similar results (not shown here) are obtained for the other decorations considered in panels (a) and (b). Shaded areas indicate the temperature ranges where only bonded configurations are identified. Insets present magnified views of the transition regime. Continuous lines are fits to $p_b(T) = [1 + e^{-(\Delta E/T - \Delta S)}]^{-1}$ within the two-state model (see text). Here, ΔE and ΔS are treated as fit parameters and are shown in Table II.

temperature is substantially lower than predicted via standard simulations in the canonical ensemble.[63,89] The states corresponding to the lower temperatures are now a result of the simulation and are not imposed by the construction of the model.[63] Moreover, we have found that at very low temperatures ($T < 0.010$), also other "unfavorable" bonded states occur (see Fig. 5) in terms of our analysis and a realistic situation, i.e., far from the transition regime, where the energetic penalty due to the bending of the strands is compensated by the attraction strength of the complementary DNA bases. Such configurations are possible for particular combinations of decoration and colloidal size, namely, for the case of a quadrangular planar geometry with $\sigma^{PP} = 2$ and an octahedral geometry with $\sigma^{PP} = 8$. In these cases, we observe the formation of two or more bonded arms. Only for these two particular cases such peculiar configurations are encountered (Fig. 5), which, however, do not cause any problem in our analysis of the effective potentials, since they appear only at very low temperatures ($T < 0.01$), i.e., far from the transition between bonded and unbonded configurations.

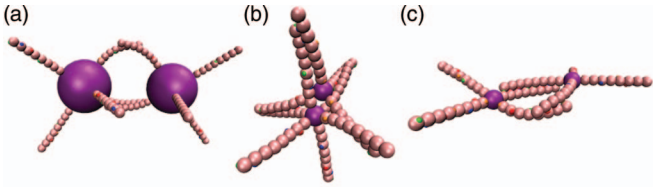

FIG. 5. At very low temperatures and for particular combinations of system parameters (i.e, the size of the colloid, the number of bases, and the geometrical decoration), we have also identified these different cases of "bonded" states. Case (a) was encountered for octahedral-octahedral decoration (o-o) and for $\sigma^{PP} = 8$. Case (b) was identified for tetrahedral-octahedral decoration (t-o) and for $\sigma^{PP} = 2$. Case (c) was encountered for tetrangular-planar decoration (c-c) and for $\sigma^{PP} = 2$. These states occur strictly for these cases of decoration and colloid size and at very low temperatures, namely, $T < 0.01$, i.e., far from the transition between bonded and unbonded configurations investigated in this study.

Our results obtained for $p_b(T)$ do not reveal any substantial effect of the decoration: two representative examples for $\sigma^{PP} = 4$ and 8 are shown in Figs. 4(a) and 4(b) for different decorations. We observe that the higher the number of DNA arms grafted onto the colloid, the higher is the probability of bonded configurations, thus, leading to higher values of $p_b(T)$ for the octahedral-octahedral case. From the results shown in Fig. 4(c), we can also clearly see the influence of the colloid size σ^{PP} on p_b: as the diameter of the colloid increases, the transition temperature between fully bonded and fully unbonded cases shifts to lower temperatures, a result that complies with previous theoretical and experimental observations.[3] By gradually increasing the size of the particles, the importance of the repulsive interaction increases steadily, thereby, hindering the bonding of the DNA strands. Whereas for colloidal diameters up to $\sigma^{PP} = 16$ we were able to obtain satisfactory data, this was not the case for colloids of size $\sigma^{PP} = 32$: In this particular case, the interaction between the colloids dominates all other interactions and hence the transition regime shifts to even smaller temperatures where it becomes considerably more difficult to sample configuration space in an efficient way with a reasonable computational effort. Since for this particular case the moves within the present approach are rather inefficient, we suggest that additional, more efficient MC moves are needed for very large values of the colloid size, i.e., when the radius of the colloidal particle becomes considerably larger than the length of the DNA strands. With these considerations in mind, we have not further considered data for a colloid size of

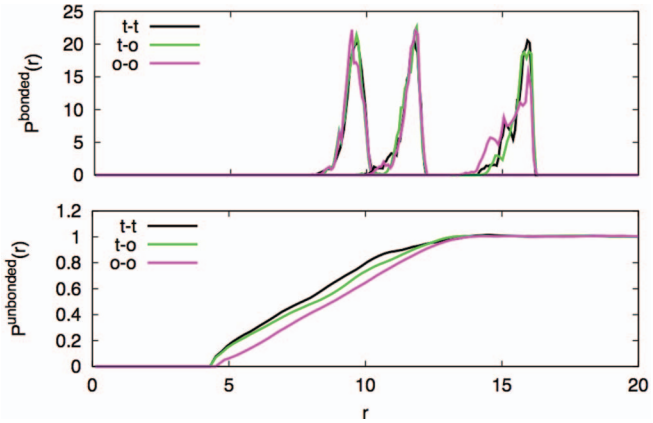

FIG. 6. $P^{\text{bonded}}(r)$ (top panel) and $P^{\text{unbonded}}(r)$ (bottom panel) as functions of r for different decoration geometries of the interacting DNA-functionalized colloids. Examples for different values of colloid size $\sigma^{\text{PP}} = 2$, 4, and 8 from left to right for the top panel and $\sigma^{\text{PP}} = 4$ for the bottom panel are shown [cf. Eq. (13) and Table II].

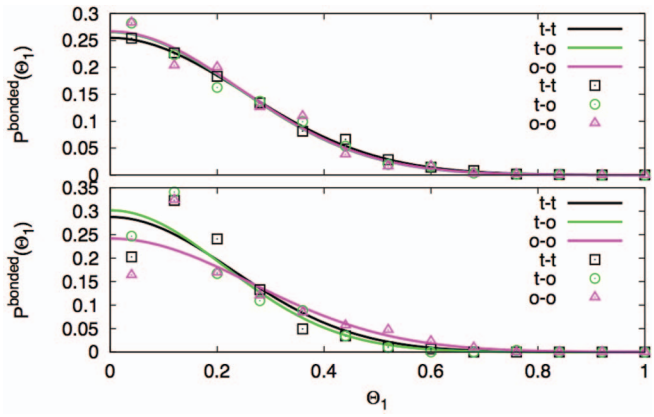

FIG. 7. $P^{\text{bonded}}(\Theta_1)$ as a function of Θ_1 (in units of rad) for different types of decoration geometries and different colloid sizes ($\sigma^{\text{PP}} = 2$ top panel and $\sigma^{\text{PP}} = 8$ bottom panel). Lines are Gaussian fits to the data points.

$\sigma^{\text{PP}} = 32$ in our study. However, we expect – in line with experimental observations[38] – a smooth extrapolation of our data with increasing particle size.

C. Evaluation of $P^{\text{bonded}}(r)$ and $P^{\text{unbonded}}(r)$

The next quantities needed for the evaluation of the effective potential are the radial distribution functions for the bonded and unbonded configurations, $P^{\text{bonded}}(r)$ and $P^{\text{unbonded}}(r)$.

In all cases investigated in the present study, the bonded configurations are realized at temperatures close to $T = 0.024$; it is therefore sufficient to calculate the function $P^{\text{bonded}}(r)$ at this temperature. We have not considered $P^{\text{bonded}}(r)$ at a lower temperature, because sampling becomes more inefficient as the temperature decreases. The results obtained for $P^{\text{bonded}}(r)$ shown in Fig. 6 display a significant dependence on the type of decoration geometry of the colloid for a given colloidal diameter σ^{PP}. When comparing our data with those obtained from standard canonical simulations[89] we observe that $P^{\text{bonded}}(r)$ obtained with parallel tempering exhibits a slightly higher peak as a result of the shift of the transition temperature to lower values ($T \approx 0.024$ compared to the original estimation[63,89] for the transition temperature at $T \approx 0.09$).

For the evaluation of $P^{\text{unbonded}}(r)$ any temperature corresponding to the unbonded case can be used; thus, we have simply used the highest temperature investigated, i.e., $T = 0.120$. Results are also shown in Fig. 6: $P^{\text{unbonded}}(r)$ vanishes at short distances depending on the size of the colloid, thus corresponding to the range of the repulsive interaction.

D. Evaluation of $P^{\text{bonded}}(\Theta_1, \Theta_2)$

The evaluation of the normalized probabilities $P^{\text{bonded}}(\Theta_1, \Theta_2) = P^{\text{bonded}}(\Theta_1)P^{\text{bonded}}(\Theta_2)$ requires a significant computational effort in order to sample different angles in the bonded states adequately. In Fig. 7, we show typical results for this $P^{\text{bonded}}(\Theta_1)$ for different decoration geometries and for two selected values of the colloidal size, $\sigma^{\text{PP}} = 2$ and $\sigma^{\text{PP}} = 8$. The distributions shown in Fig. 7 exhibit rather small variations as the colloid size increases. Also, the decoration geometry plays a rather minor role in the width of $P^{\text{bonded}}(\Theta_1)$ in the bonded case; only for the o-o decoration and for colloid size $\sigma^{\text{PP}} = 8$ we only see a more pronounced difference as our data deteriorate with increasing colloid size. We compile the results for the Gaussian fits for the normalized distribution of angle Θ_1 in Table II.

E. Evaluation of $\beta V^{\text{eff}}(r, \Theta_1, \Theta_2)$

We have now all the ingredients required for the calculation of the effective potential $\beta V^{\text{eff}}(r, \Theta_1, \Theta_2)$ via Eq. (15), as shown in Fig. 8 for various representative examples.

Figure 8(a) presents the effective interaction for different values of the colloidal size for the t-t type decoration. Not surprisingly, an increase of colloid size leads to a shift of the attractive region of the potential to larger distances. As the colloid size increases, we observe, in addition, that the attractive well at fixed temperature (e.g., $T = 0.024$) becomes shallower, i.e., further evidence that the repulsive interaction of the colloid plays an increasingly important role. Variation of the temperature T affects the depth of the attractive well,

TABLE II. The upper panel shows the values of the parameters A and s for the Gaussian fit of $P^{\text{bonded}}(\Theta_1)$ [cf. Eq. (12)]. The lower panel shows the values of the parameters ΔE (in units of $\varepsilon^{\alpha\beta}$, $\varepsilon^{\alpha\beta} = 1$) and ΔS [in units of k_B ($k_B = 1$)] of the two-state model, which was used to fit the probability of bonded configurations $p_b(T)$ [cf. Eq. (17)].

	A			s		
Decoration	$\sigma^{\text{PP}} = 2$	$\sigma^{\text{PP}} = 4$	$\sigma^{\text{PP}} = 8$	$\sigma^{\text{PP}} = 2$	$\sigma^{\text{PP}} = 4$	$\sigma^{\text{PP}} = 8$
t-t	0.159	0.163	0.165	0.249	0.247	0.229
t-o	0.159	0.157	0.161	0.239	0.214	0.213
o-o	0.160	0.151	0.160	0.240	0.247	0.264
	ΔE			ΔS		
Decoration	$\sigma^{\text{PP}} = 2$	$\sigma^{\text{PP}} = 4$	$\sigma^{\text{PP}} = 8$	$\sigma^{\text{PP}} = 2$	$\sigma^{\text{PP}} = 4$	$\sigma^{\text{PP}} = 8$
t-t	0.510	0.497	0.491	12.56	12.97	12.99
t-o	0.514	0.467	0.496	12.73	11.99	13.22
o-o	0.486	0.486	0.526	12.10	12.25	13.64

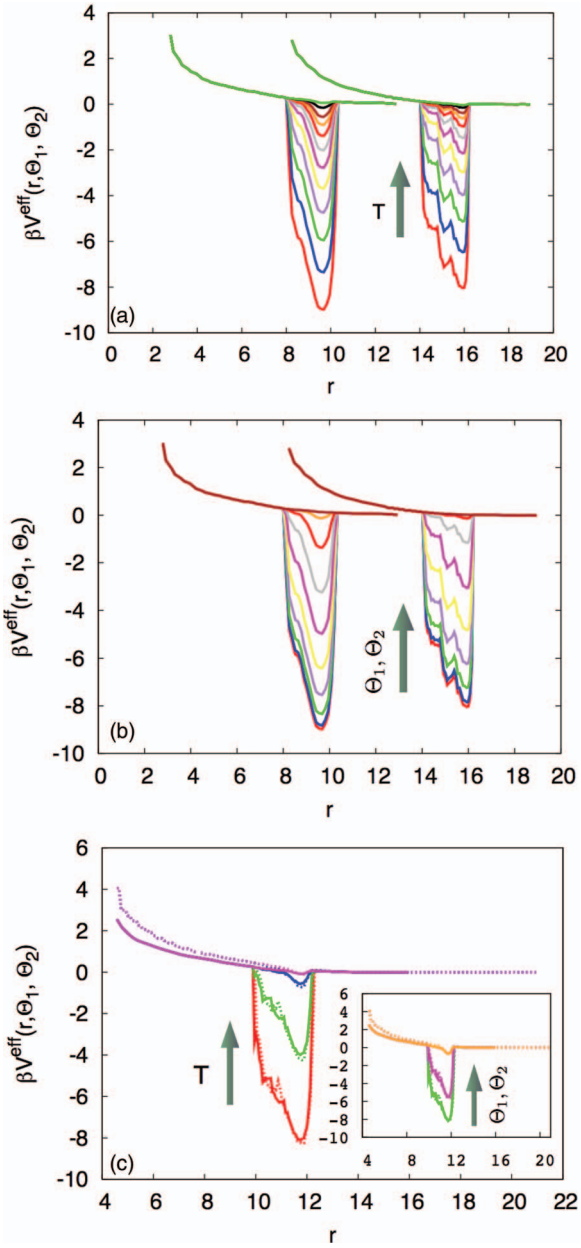

FIG. 8. The effective potential $\beta V^{\rm eff}(r, \Theta_1, \Theta_2)$ as a function of r for different system parameters. Panel (a): Results for $\sigma^{\rm PP} = 2$ and 8 for t-t decoration with $\Theta_1 = \Theta_2 = 0$ are shown. The arrow indicates the variation of the effective potential with increasing temperature (temperatures considered here are $T = 0.024$, 0.026, 0.028, 0.030, 0.032, 0.034, 0.036, 0.038, 0.040, 0.042, 0.046, and 0.052). Panel (b): Effective potential for $\sigma^{\rm PP} = 2$ and 8 for a t-t type decoration. Now, $\Theta_1 = \Theta_2$ is varied and temperature is fixed at $T = 0.024$. The arrow indicates the variation of the effective potential with increasing Θ_1 (for which the following values have been considered: $\Theta_1 = \Theta_2 = 0.0$, 0.10, 0.20, ..., and 0.90; curves are only shown if they can be discriminated from each other). Panel (c): Effective potential for $\sigma^{\rm PP} = 4$ at different temperatures $T = 0.024$, 0.030, 0.040, and 0.046. Continuous lines correspond to the tetrahedral-tetrahedral (t-t) and dashed lines to the octahedral-octahedral (o-o) decoration for $\Theta_1 = \Theta_2 = 0$. The (t-o) case is not shown here for clarity. The dependence on $\Theta_1 = \Theta_2$ ($\Theta_1 = \Theta_2 = 0.00$, 0.40, and 0.70) is also displayed in the inset.

i.e., as the temperature increases, the attractive interaction becomes weaker. Although the changes in the height of the peak of $P^{\rm bonded}(r)$ with respect to decoration are rather pronounced (cf. Fig. 6), the apparent differences in the ensuing effective potentials are not so significant.

Choosing now a low temperature such that the differences in the effective interactions become more obvious (e.g., $T = 0.024$), we depicted in Fig. 8(b) the effective potential for the case of a t-t decoration for two different values of colloid size (similar as in Fig. 8(a)). Increasing the value of Θ_1 and Θ_2 ($\Theta_1 = \Theta_2$) sufficiently, transforms the potential into a purely repulsive interaction. Finally, in Fig. 8(c) we show a comparison of the effective potential for different decorations: the t-t decoration and the o-o decoration, with the t-o decoration corresponding to an intermediate situation. For a fixed size of the colloidal particle and choosing $\Theta_1^2 + \Theta_2^2 = 0$, the variation of temperature leads to small quantitative differences between the t-t and the o-o combinations. When we fix the temperature (e.g., $T = 0.024$) and vary $\Theta_1$and Θ_2, then the potential transforms rapidly to a purely repulsive potential for the o-o decoration and t-t decoration, which is a direct effect of the contribution of $P^{\rm bonded}(\Theta_1, \Theta_2)$ to the effective interaction.

IV. SUMMARY AND CONCLUSIONS

In this contribution, we have revisited a bead-spring type model[89,90] for DNA-functionalized colloidal particles, recently proposed by Starr and Sciortino[63] and have discussed in detail a computationally demanding but faithful method to calculate the effective potential acting between two decorated particles. This potential is calculated in the dilute-regime where only two DNA-coated colloids are considered; thus, three-body potentials are neglected *a priori* in the effective potential, which now provides the basis to study structure formation in larger systems of DNA-coated colloids.

We have revisited the model put forward in Ref. 63, considering three different types of decorations of the colloidal particle by ssDNA strands (quadrangular, tetrahedral, and octahedral geometry); throughout, DNA strands formed by eight bases were used, assuming the sequence ACGTACGT. Five different values for the size of the colloidal particle were assumed. Our investigations have revealed that the apparent simplicity of this model might be misleading. The transition temperature between bonded and unbonded configurations in the effective potential is controlled by the probability $p_b(T)$; from our results we found that this transition occurs at significantly lower temperatures than originally estimated. Thus, well-defined bonded structures are expected only at considerably lower temperatures, while at the same time undesired bond-formation between DNA strands is nearly perfectly suppressed. These revised results are the consequence of the fact that we have used – in contrast to the approach suggested in Ref. 89 – extensive simulations based on the parallel tempering protocol. As a result of the shift of the transition regime to lower temperatures, where fluctuations are further suppressed, also the attractive well of the effective potential becomes slightly deeper as compared to the results presented in Ref. 89. The evaluation of effective interactions for larger colloids than the ones studied here still remains a challenge for the method described in this paper.

Finally, we point out that large scale simulations where "effective" particles interact via effective potentials require the following additional condition in order to obtain exactly

the same results that one would obtain from a full coarse-grained approach (Subsection II A): exactly one bond per effective site for the "effective" particles interacting via the effective potential has to be allowed. In this way, only one link can be established between different directions of the "effective" particle.

ACKNOWLEDGMENTS

This work was financially supported by the Austrian Science Foundation (FWF) within the SFB ViCoM (Project No. F41). P.E.T. would like to thank Julio Largo for unveiling the very details of the discussed model. The authors also thank F. Sciortino and F. W. Starr for useful communications.

[1]J. C. Crocker, Nature (London) **451**, 528 (2008).
[2]A. Travesset, Science **334**, 183 (2011).
[3]N. Geerts and E. Eiser, Soft Matter **6**, 4647 (2010).
[4]C. A. Mirkin, R. L. Letsinger, R. C. Mucic, and J. J. Storhoff, Nature (London) **382**, 607 (1996).
[5]A. P. Alivisatos, Nature (London) **382**, 609 (1996).
[6]E. Katz and I. Wilner, Angew. Chem., Int. Ed. **43**, 6042 (2004).
[7]P. L. Biancaniello, A. J. Kim, and J. C. Crocker, Phys. Rev. Lett. **94**, 058302 (2005).
[8]W. B. Rogers and J. C. Crocker, Proc. Natl. Acad. Sci. U.S.A. **108**, 15687–15692 (2011).
[9]S. Linden, C. Enkrich, M. Wegener, J. F. Zhou, T. Koschny, and C. M. Soukoulis, Science **306**, 1351 (2004).
[10]J. Lee, P. Hernandez, J. Lee, A. O. Govorov, and N. A. Kotov, Nature Mater. **6**, 291 (2007).
[11]F. X. Redl, K. S. Cho, C. B. Murray, and S. O'Brien, Nature (London) **423**, 968 (2003).
[12]J. J. Urban, D. V. Talapin, E. V. Shevchenko, C. R. Kagan, and C. B. Murray, Nature Mater. **6**, 115 (2007).
[13]T. I. N. G. Li, R. Sknepnek, R. J. Macfarlane, C. A. Mirkin, and M. O. de la Cruz, Nano Lett. **12**, 2509 (2012).
[14]N. L. Rosi and C. A. Mirkin, Chem. Rev. **105**, 1547 (2005).
[15]G. A. Ozin and A. C. Arsenault, *Nanochemistry: A Chemical Approach to Nanomaterials* (Royal Society of Chemistry, Cambridge, England, 2005).
[16]D. S. Seferos, D. A. Giljohann, H. D. Hill, A. E. Prigodich, and C. A. Mirkin, J. Am. Chem. Soc. **129**, 15477 (2007).
[17]N. L. Rosi, D. A. Giljohann, C. S. Thaxton, A. K. R. Lytton-Jean, M. S. Han, and C. A. Mirkin, Science **312**, 1027 (2006).
[18]M. M. Maye, D. Nykypanchuk, D. van der Lelie, and O. Gang, J. Am. Chem. Soc. **128**, 14020 (2006).
[19]M. M. Maye, D. Nykypanchuk, D. van der Lelie, and O. Gang, Small **3**, 1678 (2007).
[20]S. J. Park, A. A. Lazarides, C. A. Mirkin, and R. L. Letsinger, Angew. Chem., Int. Ed. **40**, 2909 (2001).
[21]S. J. Park, A. A. Lazarides, J. J. Storhoff, L. Pesce, and C. A. Mirkin, J. Phys. Chem. B **108**, 12375 (2004).
[22]S. Y. Park and D. Stroud, Phys. Rev. B **67**, 212202 (2003).
[23]S. Y. Park and D. Stroud, Phys. Rev. B **68**, 224201 (2003).
[24]S. Y. Park, J. S. Lee, D. Georganopoulou, C. A. Mirkin, and G. C. Schatz, J. Phys. Chem. B **110**, 12673 (2006).
[25]O. D. Velev, Science **312**, 376 (2006).
[26]E. Strable, J. E. Johnson, and M. G. Finn, Nano Lett. **4**, 1385 (2004).
[27]D. Nykypanchuk, M. M. Maye, D. der Lelie, and O. Gang, Langmuir **23**, 6305 (2007).
[28]A. J. Kim, P. L. Biancaniello, and J. C. Crocker, Langmuir **22**, 1991 (2006).
[29]Y. Y. Pinto, J. D. Le, N. C. Seeman, K. Musier-Forsyth, T. A. Taton, and R. A. Kiehl, Nano Lett. **5**, 2399 (2005).
[30]Z. Y. Tang and N. A. Kotov, Adv. Mater. **17**, 951 (2005).
[31]J. P. Zhang, Y. Liu, Y. G. Ke, and H. Yan, Nano Lett. **6**, 248 (2006).
[32]D. Nykypanchuk, M. M. Maye, D. van der Lelie, and O. Gang, Nature (London) **451**, 549 (2008).
[33]S. Y. Park, A. K. R. Lytton-Jean, B. Lee, S. Weigand, G. C. Schatz, and C. A. Mirkin, Nature (London) **451**, 553 (2008).
[34]R. J. Macfarlane, B. Lee, H. D. Hill, A. J. Senesi, S. Seifert, and C. A. Mirkin, Proc. Natl. Acad. Sci. U.S.A. **106**, 10493 (2009).
[35]R. J. Macfarlane, M. R. Jones, A. J. Senesi, K. L. Young, B. Lee, J. S. Wu, and C. A. Mirkin, Angew. Chem., Int. Ed. **49**, 4589 (2010).
[36]M. R. Jones, R. J. Macfarlane, B. Lee, J. A. Zhang, K. L. Young, A. J. Senesi, and C. A. Mirkin, Nature Mater. **9**, 913 (2010).
[37]H. Xiong, D. van der Lelie, and O. Gang, Phys. Rev. Lett. **102**, 015504 (2009).
[38]R. J. Macfarlane, B. Lee, M. R. Jones, N. Harris, G. C. Schatz, and C. A. Mirkin, Science **334**, 204 (2011).
[39]N. Harris, M. R. Jones, R. J. Macfarlane, C. A. Mirkin, and G. C. Schatz, ACS Preprints **242**, 419-PHYS (2011).
[40]E. Auyeung, J. I. Cutler, R. J. Macfarlane, M. R. Jones, J. Wu, G. Liu, K. Zhang, K. D. Osberg, and C. A. Mirkin, Nat. Nanotechnol. **7**, 24 (2012).
[41]M.-P. Valignat, O. Theodoly, J. C. Crocker, W. B. Russel, and P. M. Chaikin, Proc. Natl. Acad. Sci. U.S.A. **102**, 4225 (2005).
[42]P. Cigler, A. K. R. Lytton-Jean, D. G. Anderson, M. G. Finn, and S. Y. Park, Nature Mater. **9**, 918 (2010).
[43]J. D. Joannopoulos, S. G. Johnson, J. N. Winn, and R. D. Meade, *Photonic Crystals: Molding the Flow of Light* (Princeton University Press, 2008).
[44]D. J. Norris, Nature Mater. **6**, 177 (2007).
[45]E. Yablonovitch, Phys. Rev. Lett. **58**, 2059 (1987).
[46]S. John, Phys. Rev. Lett. **58**, 2486 (1987).
[47]D. M. Ho, C. T. Chan, and C. M. Soukoulis, Phys. Rev. Lett. **65**, 3152 (1990).
[48]T. T. Ngo, C. M. Liddell, M. Ghebrebrhan, and J. D. Joannopoulos, Appl. Phys. Lett. **88**, 241920 (2006).
[49]A. P. Hynninen, J. H. J. Thijssen, E. C. M. Vermolen, M. Dijkstra, and A. van Blaaderen, Nature Mater. **6**, 202 (2007).
[50]D. R. Nelson, Nano Lett. **2**, 1125 (2002).
[51]A. M. Kalsin, M. Fialkowski, M. Paszewski, S. K. Smoukov, K. J. M. Bishop, and B. A. Grzybowski, Science **312**, 420 (2006).
[52]A. V. Tkachenko, Phys. Rev. Lett. **89**, 148303 (2002).
[53]H. Xing, Z. Wang, Z. Xu, N. Y. Wong, Y. Xiang, G. L. Liu, and Y. Lu, ACS Nano **6**, 802 (2012).
[54]F. Garcia-Santamaria, C. Lopez, F. Mesequer, F. Lopez-Tejeira, J. Sanchez-Dehesa, and H. T. Miyazaki, Appl. Phys. Lett. **79**, 2309 (2001).
[55]F. Garcia-Santamaria, H. T. Miyazaki, A. Urquia, M. Ibisate, M. Belmonte, N. Shinya, F. Meseguer, and C. Lopez, Adv. Mater. **14**, 1144 (2002).
[56]T. E. Ouldridge, A. A. Louis, and J. P. K. Doye, Phys. Rev. Lett. **104**, 178101 (2010).
[57]T. E. Ouldridge, A. A. Louis, and J. P. K. Doye, J. Chem. Phys. **134**, 085101 (2011).
[58]R. T. Scarlett, J. C. Crocker, and T. Sinno, J. Chem. Phys. **132**, 234705 (2010).
[59]M. E. Leunissen and D. Frenkel, J. Chem. Phys. **134**, 084702 (2011).
[60]B. M. Mognetti, M. E. Leunissen, and D. Frenkel, Soft Matter **8**, 2213 (2012).
[61]M. Sales-Pardo, R. Guimera, A. A. Moreira, J. Widom, and L. A. N. Amaral, Phys. Rev. E **71**, 051902 (2005).
[62]M. Kenward and K. D. Dorfman, J. Chem. Phys. **130**, 095101 (2009).
[63]F. W. Starr and F. Sciortino, J. Phys.: Condens. Matter **18**, L347 (2006).
[64]K. Drukker, G. Wu, and G. C. Schatz, J. Chem. Phys. **114**, 579 (2001).
[65]E. J. Sambriski, V. Ortiz, and J. J. de Pablo, J. Phys.: Condens. Matter **21**, 034105 (2009).
[66]E. J. Sambriski, D. C. Schwartz, and J. J. de Pablo, Biophys. J. **96**, 1675 (2009).
[67]D. B. Lukatsky and D. Frenkel, Phys. Rev. Lett. **92**, 068302 (2004).
[68]D. B. Lukatsky, and D. Frenkel, J. Chem. Phys. **122**, 214904 (2005).
[69]D. B. Lukatsky, B. M. Mulder, and D. Frenkel, J. Phys.: Condens. Matter **18**, S567 (2006).
[70]F. J. Martinez-Veracoechea, B. M. Mladek, A. V. Tkachenko, and D. Frenkel, Phys. Rev. Lett. **107**, 045902 (2011).
[71]F. J. Martinez-Veracoechea, B. Bozorgui, and D. Frenkel, Soft Matter **6**, 6136 (2010).
[72]C. Knorowski, S. Burleigh, and A. Travesset, Phys. Rev. Lett. **106**, 215501 (2011).
[73]M. C. Linak, R. Tourdot, and K. D. Dorfman, J. Chem. Phys. **135**, 205102 (2011).
[74]G. S. Grest and K. Kremer, Phys. Rev. A **33**, 3628 (1986).
[75]K. Kremer and G. S. Grest, J. Chem. Phys. **92**, 5057 (1990).
[76]P. E. Theodorakis and N. G. Fytas, Soft Matter **7**, 1038 (2011).
[77]P. E. Theodorakis, W. Paul, and K. Binder, EPL **88**, 63002 (2009).

[78]P. E. Theodorakis, W. Paul, and K. Binder, Macromolecules **43**, 5137 (2010).
[79]P. E. Theodorakis, W. Paul, and K. Binder, J. Chem. Phys. **133**, 104901 (2010).
[80]P. E. Theodorakis, H.-P. Hsu, W. Paul, and K. Binder, J. Chem. Phys. **135**, 164903 (2011).
[81]I. Erukhimovich, P. E. Theodorakis, W. Paul, and K. Binder, J. Chem. Phys. **134**, 054906 (2011).
[82]N. G. Fytas and P. E. Theodorakis, J. Phys.: Condens. Matter **23**, 235106 (2011).
[83]P. E. Theodorakis and N. G. Fytas, EPL **93**, 43001 (2011).
[84]H. Maleki and P. E. Theodorakis, J. Phys.: Condens. Matter **23**, 505104 (2011).
[85]P. E. Theodorakis, W. Paul, and K. Binder, Eur. Phys. J. E **34**, 52 (2011).
[86]P. E. Theodorakis and N. G. Fytas, J. Chem. Phys. **136**, 094902 (2012).
[87]M. T. Horne, D. J. Fish, and A. S. Benight, Biophys. J. **91**, 4133 (2006).
[88]B. Tinland, A. Pluen, J. Sturm, and G. Weill, Macromolecules **30**, 5763 (1997).
[89]J. Largo, P. Tartaglia, and F. Sciortino, Phys. Rev. E **76**, 011402 (2007).
[90]J. Largo, private communication (2011).
[91]J. Largo, F. W. Starr, and F. Sciortino, Langmuir **23**, 5896 (2007).
[92]C. W. Hsu, J. Largo, F. Sciortino, and F. W. Starr, Proc. Natl. Acad. Sci. U.S.A. **105**, 13711 (2008).
[93]W. Dai, C. W. Hsu, F. Sciortino, and F. W. Starr, Langmuir **26**, 3601 (2010).
[94]C. W. Hsu, F. Sciortino, and F. W. Starr, Phys. Rev. Lett. **105**, 055502 (2010).
[95]W. Dai, S. K. Kumar, and F. W. Starr, Soft Matter **6**, 6130 (2010).
[96]F. V. Lara and F. W. Starr, Soft Matter **7**, 2085 (2011).
[97]O. Padovan-Merhar, F. V. Lara, and F. W. Starr, J. Chem. Phys. **134**, 244701 (2011).
[98]M. E. J. Newman and G. T. Barkema, *Monte Carlo Methods in Statistical Physics* (Oxford University Press, New York, 1999).
[99]*Monte Carlo and Molecular Dynamics Simulations in Polymer Science*, edited by K.Binder (Oxford University Press, New York, 1995).
[100]R. Auhl, R. Everaers, G. S. Grest, K. Kremer, and S. J. Plimpton, J. Chem. Phys. **119**, 12718 (2003).
[101]M. Tsige, T. R. Mattsson, and G. S. Grest, Macromolecules **37**, 9132 (2004).
[102]J. D. Watson, T. A. Baker, S. P. Bell, A. Gann, M. Levine, and R. Losick, *Molecular Biology of the Gene*, 5th ed. (Pearson Benjamin Cummings, 2004).
[103]L. Feng, R. Sha, N. C. Seeman, and P. M. Chaikin, Phys. Rev. Lett. **109**, 188301 (2012).
[104]N. Metropolis and S. Ulam, J. Am. Stat. Assoc. **44**, 335 (1949).
[105]R. H. Swendsen and J.-S. Wang, Phys. Rev. Lett. **57**, 2607 (1986).
[106]C. J. Geyer, "Computing science and statistics," in *Proceedings of the 23rd Symposium on the Interface* (American Statistical Association, New York, 1991), p. 156.
[107]D. J. Earl and M. W. Deem, Phys. Chem. Chem. Phys. **7**, 3910 (2005).
[108]Y. Sugita and Y. Okamoto, Chem. Phys. Lett. **314**, 141 (1999).
[109]D. A. Kofke, J. Chem. Phys. **117**, 6911 (2002).
[110]D. A. Kofke, J. Chem. Phys. **120**, 10852 (2004).
[111]V. I. Manousiouthakis and M. W. Deem, J. Chem. Phys. **110**, 2753 (1999).